





Optical Inclinometer Based on a LPG-Taper Series Configuration

Renato Luiz Faraco Filho¹ , Alexandre Bessa dos Santos² , Andrés Pablo López Barbero³ ,
Vinicius Nunes Henrique Silva³ 

¹Universidade Federal de Juiz de Fora/UFJF, Juiz de Fora, Brazil,
renato.luiz@engenharia.ufjf.br

²Departamento de Circuitos Elétricos, Universidade Federal de Juiz de Fora/UFJF, Juiz de Fora, Brazil,
alexandre.bessa@engenharia.ufjf.br

³Departamento de Engenharia de Telecomunicações, Universidade Federal Fluminense/UFF, Niterói, Brazil,
lopez.barbero@gmail.com, viniciusnhs@id.uff.br

Abstract— This article presents the development of an inclinometer device based on a Mach-Zehnder interferometer considering the effects caused by temperature variations. It was demonstrated the operation of a LPG-taper system for angle measurements. The practical results satisfactorily show reliable inclination measures, even with the cross sensibility effect caused by variable temperature.

Index Terms— calibration, inclination, interferometer, LPG, taper.

I. INTRODUCTION

Long period gratings (LPG) are optical devices that couple the forward-propagating guided mode to forward propagating cladding modes of a single-mode optical fiber, leaving a set of attenuation bands in the transmission spectrum [1]. This forward coupling is obtained by a periodic refractive index modulation of a hundred micrometers along with the core of the optical fiber [2]. Its use as a sensor occurs because of its central wavelength, denoted by λ_{res}^m , and it is function of surroundings variable parameters. These parameters are: the core refractive index ($n_{eff,co}$), the effective refractive index of the m-th cladding mode ($n_{eff,cl}^m$) and the modulation period Λ of the LPG [3], [4]. This relation is quoted by:

$$\lambda_{res}^m = (n_{eff,co} - n_{eff,cl}^m) \cdot \Lambda \quad (1)$$

As they are optical fiber-built devices, these sensors are appropriate for remote sensing applications, due to the ease of transmission via an optical link and the low signal attenuation in these apparatus. Furthermore, these sensors are light, compacts, and immune to electromagnetic interference and oxidation, occasioning them ideal for measurements near high magnetic fields such as transmission lines and large turbines used in electrical energy generation [5].

Moreover, LPGs can equally be used to implement versatile fiber-mode interferometers with enhanced parameter sensitivity [1]. This is done either by cascading two similar LPGs within a certain fiber length resulting in a single-fiber Mach-Zehnder configuration [6], [7], or by employing a single LPG and a mirror, resulting in a Michelson interferometer [8], [9].

Another topology for the Mach-Zehnder interferometer elaboration can be developed by the combination of a uniquely long period grating and a fused taper. Its operating principle is based on the fact that the taper couples a fraction of the core light to the cladding modes, and then, the LPG positioned some distance after the taper, recouples the light in the cladding modes into the fiber core [2].

It is substantial to emphasize that the quoted topology in the previous paragraph allows the realization of more versatile tests, once the taper on the system provides punctual flexibility that cannot be found in other configurations. A quantitative manner to determine the quality or contrast of the interference patterns is calculating the interferometric visibility [2], $v(r)$, function of the maximum intensity of the oscillations (I_{max}), the minimum intensity of the oscillations (I_{min}).

$$v(r) = \frac{I_{max} - I_{min}}{I_{max} + I_{min}} \quad (2)$$

Additionally, it is important to highlight that the interferometric visibility represents an absolute parameter, so, there is no need for any kind of referentiation, becoming a relevant feature of the system [2]. In this context, it is possible to realize tests that need some system malleability, e.g. inclination measures.

II. METHODOLOGY

A. Devices manufacturing

Initially, it was developed a LPG sensor from a single mode optical fiber SMF-28, using the electrical arcs technique described by Rego et al. [10]. The LPG used in this experiment had a period of $\Lambda = 500 \mu\text{m}$ and a total diffraction grating length of 17 mm, totaling 34 electrical discharges, realized by 110 bits (manufacturer unit) electrical arc power, and a discharge time of 10 ms. The optical fiber fusion splicer used in this experiment was the Jilong KL-330T.

The sensor transmitted spectrum, in air, ambient temperature (21 °C), and no deformations, had a fixed wavelength of 1508 nm and an attenuation of 5 dB, and the spectrum can be seen in Fig. 1. Afterwards, it was manufactured a taper from a single-mode fiber SMF-28 through the stretching of the optical fiber during a unique electric discharge. The arc power settings used in the taper manufacturing were a power of 110 bits and a discharge time of 2 seconds. The parameters of the manufactured taper are the cladding reduction from 125 μm to 82.5 μm and a total length of approximately 1500 μm .

The curve related to the ELED source is represented by the spectrum that does not have attenuation valleys. Its characteristic aspect is due to the high spectral width of the ELED sources, presenting higher power in the central wavelength and lower powers in the extremity wavelengths. The curve related to the Long Period Grating is represented by the spectrum that has a single attenuation valley. Its characteristic aspect is due to the couple of the forward-propagating guided modes to forward propagating cladding modes of a single-mode optical fiber, leaving an attenuation dip in a certain wavelength range of the transmission spectrum. The curve related to the interferometer is represented by the spectrum that has multiple attenuation dips. Its characteristic is due to the fact that typically an incident light beam of the interferometer is split into two or more parts and then recombined together to create an interference pattern, allowing the visualization of fringes in the spectrum.

For all three obtained spectra, an ELED light source and an optical spectrum analyzer (OSA) were used. Initially, the ELED source was connected directly to the OSA for the obtainment of its characteristic spectrum. Second, a Long Period Grating was spliced between the light source and the OSA, for the obtainment of its curve. Subsequently, a tapered optical fiber was positioned between the LPG and the ELED light source, for the obtainment of the interferometer characteristic curve.

After the fabrication of the two instruments, a splice was made between the taper and the LPG with a distance of approximately 40 mm. The spectra is presented in Fig. 1. Moreover, the channeled

spectrum contains an approximately 10 nm fringe periodicity.

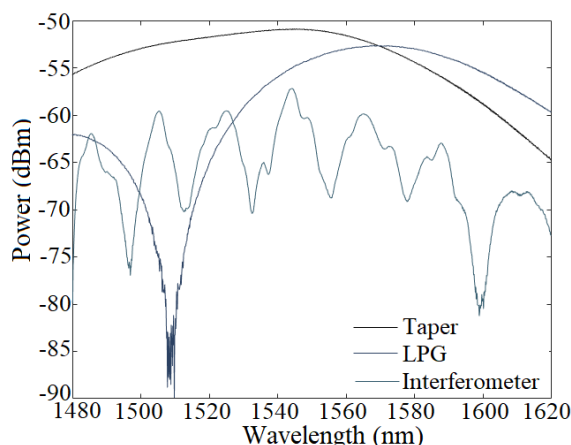


Fig. 1. Obtained spectra during the interferometer manufacturing.

B. Temperature tests

The interferometer was positioned in a way that the fiber was completely straight on the workbench at a slope of 0° . Subsequently, the system was submitted to seven different temperatures for 3 rounds, for obtaining the calibration curve.

For the temperature variation in the device, it was employed a handheld hot air gun, and the incident heat flux on the LPG-taper set caused a punctual temperature change in the system. It also was employed a "j" type thermocouple with an uncertainty of $\pm 1^\circ\text{C}$ as a reference sensor, for obtaining the temperature of the collected spectra. A total of 21 spectral curves was pre-processed by Savitzky-Golay filters. The selected window size was 41 and the chosen order was 10.

After the signal filtering, the wavelength variations of each fringe were extracted and associated with its respective temperatures measured by the reference sensor. Therefore, the calibration curve was obtained by the linear adjustment to these experimental points.

C. Inclination tests

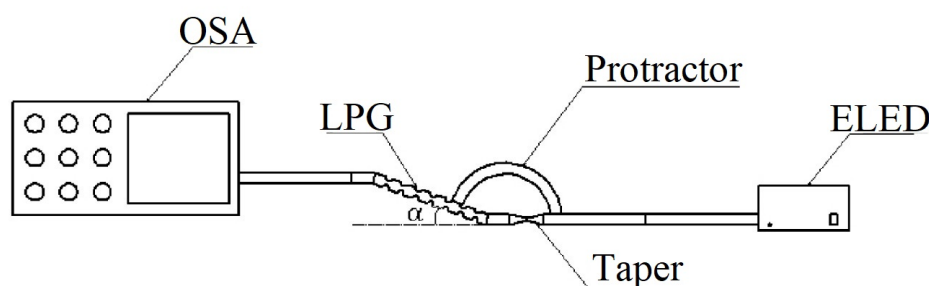


Fig. 2. System diagram for the inclination tests.

For the slope variation tests, the interferometer was positioned between two trapezoidal plates manufactured by a Replicator Z18 3D printer. The LPG was on top of one of the plates, and the taper was on the interspace between the two plates. Figure 2 shows the elaborated system and Fig. 3

presents the realized experiment. Posteriorly, the system was submitted to six different angles for six rounds, for obtaining the calibration curve.

For the angle variation, were used metal washers of identical dimensions to increase the height of one of the plates in a uniform way. The washers were positioned under the LPG plate, resulting in slope variation. A protractor with an uncertainty of $\pm 1^\circ\text{C}$ was used as a calibration reference for the obtained angles. A total of 36 spectral curves was pre-processed by Savitzky-Golay filters. The selected window size was 41 and the chosen order was 10.

After the signal filtering, the wavelength variations of each fringe and the fringe visibility were extracted and associated with its respective tilt angles measured by the protractor. Therefore, the calibration curve was obtained by the polynomial adjustment to these experimental points, because of nonlinearities found in the obtained data.

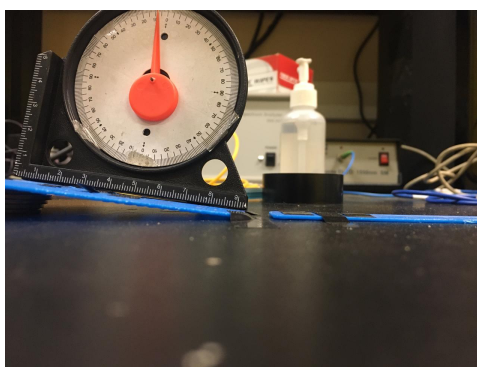


Fig. 3. Inclination tests performed in laboratory.

D. Sensor behavior over time analysis

After the proper calibration, the system was maintained at a 0° slope in a workbench at a 15.1°C temperature for 30 minutes, engendering a total of approximately 330 collected spectra. Afterward, the workbench was contained at the same temperature, the system slope was raised to 8° and the spectra were collected for 30 minutes.

Then, the sensor was maintained at an inclination of 0° , the workbench temperature was increased to 21.3°C and were collected approximately 330 spectra. Subsequently, the workbench was kept at the same temperature, and the system slope was increased to 8° . The spectra were obtained according to the previous stages.

III. RESULTS

A. Temperature tests results

During the calibration the interferometer was kept at the temperatures indicated in Table I, and all measurements present uncertainty of $\pm 1^\circ\text{C}$. The obtained spectra in each test can be examined in Fig. 4, and the collected temperatures can be seen in Table I.

After the wavelength extraction of every fringe, for each collected spectrum. The average temperature value, as well as the respective wavelength values, were calculated and can be seen in Fig. 5. It equally can be noted the calibration curve. The error bars in the y-axis represent the resonant wavelength variation, and the error bars in the x-axis represent the temperature variations in each test. It is substantial to emphasize that the calibration curves were plotted for all fringes presented in the optical spectrum, however, the shown curve in this paper refers to the best-obtained result.

TABLE I. TEMPERATURES USED FOR CALIBRATION (°C)

Experiment 1	Experiment 2	Experiment 3
22.5	22.9	22.3
23.1	23.5	23.3
24.7	24.2	24.9
25.5	26.0	25.7
27.3	27.1	27.6
30.2	29.9	30.4
31.3	31.6	30.8

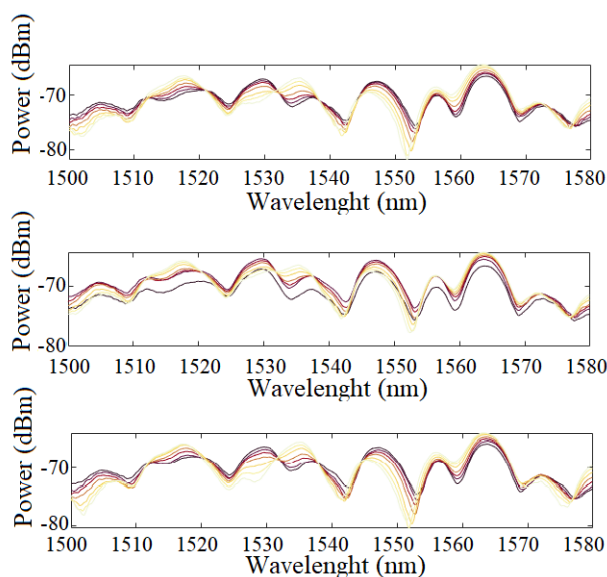


Fig. 4. Obtained spectra during temperature tests.

The linear and angular coefficients of the curve can be found in Table II, and the coefficient of determination of the curve is $R^2 = 0.9909$.

TABLE II. CALIBRATION CURVE COEFFICIENTS

Linear coefficient	Angular coefficient
1467.5	0.35966

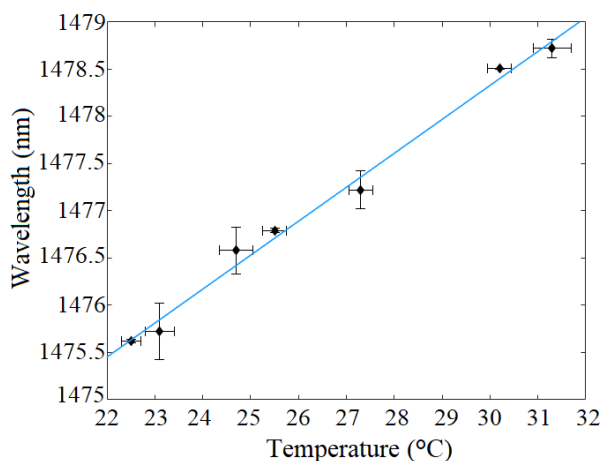


Fig. 5. Calibration curve for the temperature test.

B. Inclination tests results

During the calibration, the system was maintained at the following angles: 0°; 1°; 3°; 4°; 7°; 8°. All the measurements present uncertainty of $\pm 0.5^\circ$, and it is important to emphasize the angles for all the experiments were the same, once the washers used for the slope variations were the same and were positioned at the same order. The obtained spectra in each test can be examined in Fig. 6.

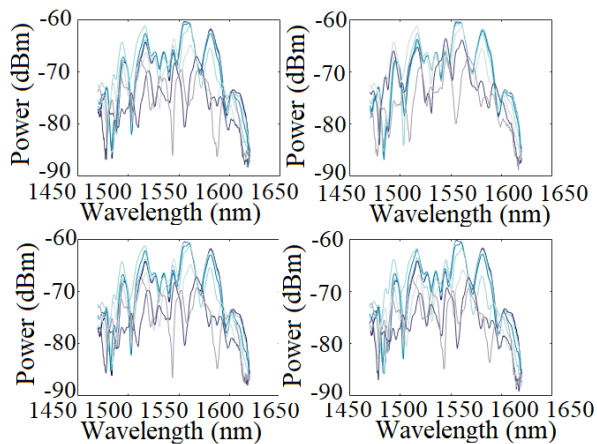


Fig. 6. Obtained spectra during inclination tests.

After the extraction of all the wavelengths of all fringes presented in the optical signal for each spectrum collected, the typical value of the inclination obtained during the tests as well as the average values of the respective wavelengths, were calculated and they can be seen in Fig. 7. The error bars in the y-axis represent the resonant wavelengths variations, and the x-axis represents the inclination variations. The curve equation referring to the resonant wavelength is shown in (3), α is the slope

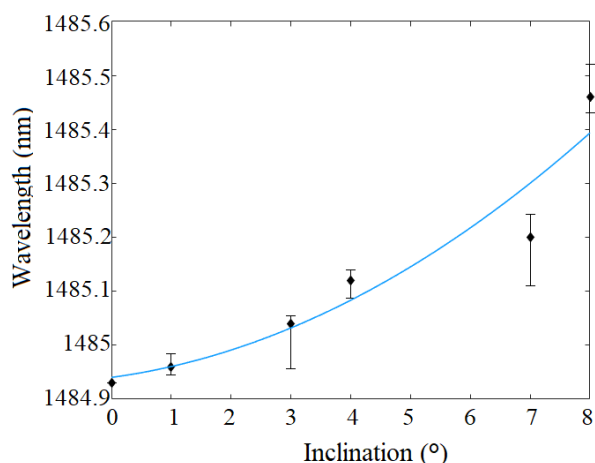


Fig. 7. Calibration curve for inclination sensing, considering the resonant wavelength.

angle, λ is the wavelength, and the determination coefficient of the curve is $R^2 = 0.9158$.

$$\lambda = 0.0052182\alpha^2 + 0.014895\alpha + 1484.9 \quad (3)$$

Furthermore, the calibration curve for interferometric visibility can be seen in Fig. 8. The error bars in the y-axis represent the interferometric visibility variations, and the x-axis represent the inclination variations in each test.

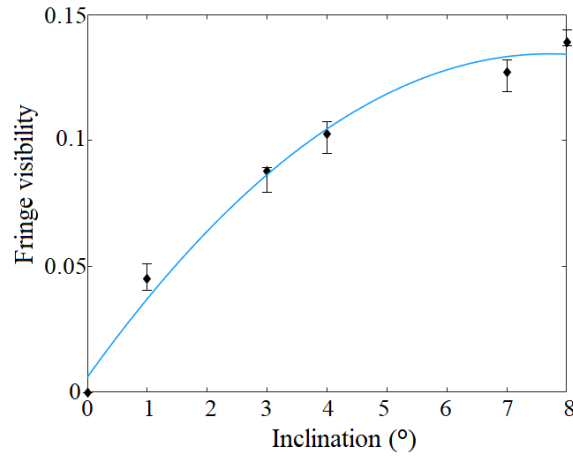


Fig. 8. Calibration curve for inclination sensing, considering the fringe visibility.

The curve equation referring to the fringe visibility is shown in (4), α is the slope angle and v is the visibility, the coefficient of determination of the curve is $R^2 = 0.9879$.

$$v = -0.0021549\alpha^2 + 0.033265\alpha + 0.0059753 \quad (4)$$

C. Sensor behavior over time results

From the obtained results, it was feasible to plot a histogram presented in Fig. 9, on the y-axis it is possible to note the probability density, and on the x-axis, it is possible to observe the measured inclination. Plus, analyzing the obtained results, it is possible to conclude that the histograms tend to a Gaussian probability density function. This function was estimated by the residual average and the standard deviation. The calculated values are presented in Table III.

TABLE III. CALCULATED VALUES FOR RESIDUAL AVERAGE AND STANDARD DEVIATION

Temperature	Residual average μ	Standard deviation σ
15.1	0.0388	0.0047
21.3	0.0033	0.0058

It is pertinent to emphasize that is possible to observe, in Fig. 9, the cross-sensitivity effect generated by temperature, since there is a discrepancy between the obtained histograms at the same inclination and different temperatures.

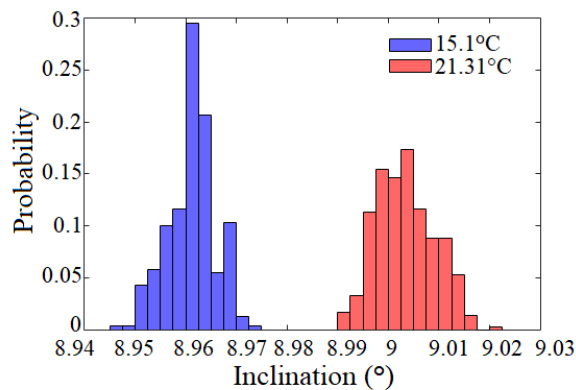


Fig. 9. Histograms related to inclination variations obtained in two different temperatures.

Moreover, the temporal results of the measurements at 9° and temperatures of $15,1^\circ$ e $21,3^\circ$ are shown in Fig. 10.

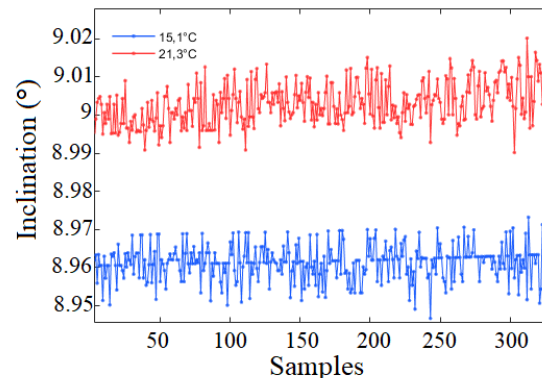


Fig. 10. Temporal series obtained for inclination variations in two different temperatures.

IV. CONCLUSION

In this article, the aim of the experiments was to design an optical inclinometer based on a Mach-Zehnder interferometer in a LPG-taper series configuration. The device was capable of identifying the angular variation presented by the analyzed surface, despite the effects caused by temperature variations.

Through the obtained data analysis were observed nonlinear changes in the spectrum occasioned by angular variations of the analyzed surface. Furthermore, expressive wavelength displacements caused by temperature changes were identified, making it possible to visualize cross-sensitivity effects.

Those are relevant features for the following experiments, which will test the structural health monitoring resources of the device since the deformation suffered by the inclinometer allows a more proper recognition of structural bendings of the analyzed structure.

ACKNOWLEDGEMENT

The authors thank the support from the Programa de Pós-graduação em Engenharia Elétrica (PPEE-UFJF), Pró-Reitoria de Pós-Graduação e Pesquisa da UFJF, Coordenação de Aperfeiçoamento Pessoal de Nível Superior (CAPES), Conselho Nacional de Desenvolvimento Científico e Tecnológico (CNPq), Instituto Nacional de Energia Elétrica (Inerge-UFJF), Fapemig and Transmissoras Brasileiras de Energia (TBE).

REFERENCES

- [1] A. M. Vengsarkar, "Long-period fiber gratings as band-rejection filters," *Journal of Lightwave Technology*, vol. 14, no. 1, pp. 58–65, 1996.
- [2] O. Frazão, "Optical inclinometer based on a single long-period fiber grating combined with a fused tape," *Optical Letters*, vol. 31, no. 20, pp. 459–512, 2006.
- [3] T. Erdogan, "Fiber grating spectra," *Journal of Lightwave Technology*, vol. 15, no. 8, pp. 1277–1294, 1997.
- [4] X. Shu, "Sensitivity characteristics of long-period fiber gratings," *Journal of Lightwave Technology*, vol. 20, no. 2, pp. 255–266, 2002.
- [5] F. O. Barino and A. B. dos Santos, "Sensor óptico LPFG para avaliação de forças bidirecionais," *XXII Congresso Brasileiro de Automática*, vol. 1, no. 1, 2019.
- [6] Y. Liu, "Phase shifted and cascaded long-period fiber gratings," *Optics Communications*, vol. 164, no. 1-3, pp. 27–31, 1999.

- [7] Y. G. Han, "Fibre-optic sensing applications of a pair of long-period fibre gratings," *Measurement Science and Technology*, vol. 12, no. 7, pp. 778–781, 2001.
- [8] B. H. Lee and J. Nishii, "Self-interference of long-period fibre grating and its application as temperature sensor," *Electronics Letters*, vol. 34, no. 21, pp. 2059–2060, 1998.
- [9] P. L. Swart, "Long-period grating Michelson refractometric sensor," *Measurement Science and Technology*, vol. 15, no. 8, pp. 1576–1580, 2004.
- [10] G. Rego, "Arc-induced long-period gratings," *Fiber and Integrated Optics*, vol. 24, no. 3-4, pp. 245–259, 2005.
- [11] R. A. P. Herrera, "Multiplexing optical fiber fabry-perot interferometers based on air-microcavities," *Proceedings Of SPIE*, vol. 11199, no. 78, 2019.
- [12] R. P. Murphy, "Multiplexing of fiber-optic long-period grating based interferometric sensors," *Journal of Lightwave Technology*, vol. 25, no. 3, pp. 825–829, 2007.
- [13] B. H. Lee, "Interferometric fiber optic sensors," *Sensors*, vol. 12, no. 3, pp. 2467–2486, 2012.
- [14] Z. Tian, "In-line single-mode optical fiber interferometric refractive index sensors," *Journal of Lightwave Technology*, vol. 27, no. 13, pp. 2296–2306, 2009.
- [15] Z. Tian, "In-line abrupt taper optical fiber mach-zehnder interferometric strain sensor," *IEEE Photonics Technology Letters*, vol. 21, no. 3, pp. 161–163, 2009.
- [16] D. W. Kim, "In-fiber reflection mode interferometer based on a long-period grating for external refractive-index measurement," *Applied Optics*, vol. 44, no. 26, pp. 5368–5373, 2005.
- [17] L. Alwis, "Fibre optic long period grating-based humidity sensor probe using a michelson interferometric arrangement," *Sensors and Actuators*, vol. 178, no. 1, pp. 694–699, 2013.
- [18] C.-L. Lee, Jen-Te Chao and P. Han., "Dual taper-shaped polymers fiber mach-zehnder interferometer," in *2019 24th OptoElectronics and Communications Conference (OECC) and 2019 International Conference on Photonics in Switching and Computing (PSC)*, 2019.
- [19] O. Frazão, "All-fiber mach-zehnder curvature sensor based on multimode interference combined with a long-period grating," *Optics Letters*, vol. 32, no. 21, pp. 3074–3076, 2007.
- [20] J. H. Osório, "All-fiber mach-zehnder curvature sensor based on multimode interference combined with a long-period grating," *Measurement Science and Technology*, vol. 24, no. 1, 2013.
- [21] J. Li, "A compact fiber inclinometer using a thin-core fiber with incorporated an air-gap microcavity fiber interferometer," *Sensors*, vol. 16, no. 1, 2016.
- [22] L. M. N. Amaral, "Optical inclinometer based on fibre-taper-modal michelson interferometer," *Proceedings of SPIE*, vol. 7653, 2010.
- [23] T. Allsop, "Tapered fibre LPG device as a sensing element for refractive index," *Proceedings Of SPIE*, vol. 5855, 2013.
- [24] J.-F. Ding, "Fiber-taper seeded long-period grating pair as a highly sensitive refractive-index sensor," *IEEE Photonics Technology Letters*, vol. 17, no. 6, pp. 1247–1249, 2005.
- [25] P. Caldas, "Effect of fiber tapering in LPG-based mach-zehnder modal interferometers for refractive-index sensing," *Proceedings Of SPIE*, vol. 7503, 2009.